5-2008

Tendinopathy Discrimination by Use of Spatial Frequency Parameters in Ultrasound B-Mode Images

Gregory R. Bashford
University of Nebraska - Lincoln, gbashford2@unl.edu

Nicholas Tomsen
University of Iowa

Shruti Arya
University of Southern California

Judith M. Burnfield
Institute for Rehabilitation Science and Engineering, jburnfield@madonna.org

Kornelia Kulig
University of Southern California

Tendinopathy Discrimination by Use of Spatial Frequency Parameters in Ultrasound B-Mode Images

Gregory R. Bashford*, *Senior Member, IEEE*, Nicholas Tomsen, Shruti Arya, Judith M. Burnfield, and Kornelia Kulig

***Abstract*—The structural characteristics of a healthy tendon are related to the anisotropic speckle patterns observed in ultrasonic images. This speckle orientation is disrupted upon damage to the tendon structure as observed in patients with tendinopathy. Quantification of the structural appearance of tendon shows promise in creating a tool for diagnosing, prognosing, or measuring changes in tendon organization over time. The current work describes a first step taken towards this goal—classification of Achilles tendon images into tendinopathy and control categories. Eight spatial frequency parameters were extracted from regions of interest on tendon images, filtered and classified using linear discriminant analysis. Resulting algorithms had better than 80% accuracy in categorizing tendon image kernels as tendinopathy or control. Tendon images categorized wrongly provided for an interesting clinical association between incorrect classification of tendinopathy kernels as control and the symptom and clinical time history based inclusion criteria. To assess intersession reliability of image acquisition, the first 10 subjects were imaged twice during separate sessions. Test-retest of repeated measures was excellent ($r = 0.996, \mathrm{ICC}\ (2,1) = 0.73$ with one outlier) indicating a general consistency in imaging techniques.**

***Index Terms*—Classifier, image analysis, tendinopathy, tendon, ultrasound.**

I. Introduction

STRUCTURAL organization of connective tissue is influenced by its functional role and the presence of pathology [1]. Tendons are designed to transfer loads from muscle to bone, hence their primary organization is in the form of a parallel array of collagen bundles that are aligned in the direction of the tensile force [1]. This structural design is evidenced on ultrasound images in the form of an anisotropic speckle pattern [assuming an isotropic imaging point spread function (PSF)], consisting of parallel striations with longer correlation length in the direction of the collagen bundles than in the direction normal to the collagen bundles. This characteristic pattern makes the tendon easily distinguishable from other tissues. Trauma, arising from an excessive rate or magnitude of loading, can disturb the unique pattern of collagen bundle organization [2], [3]. Clinically, this can lead to the development of a tendinopathy as evidenced by the presence of pain and functional limitation for periods longer than six weeks, without relief from anti-inflammatory medication. The accompanying disruption of tissue organization results in a more isotropic speckle pattern, with visual analysis suggesting reduced organization of the parallel striations and localized regions of hypoechogenicity [4]–[7]. It has been shown that changes in ultrasound radio-frequency (RF) spectra may be used to indicate damage in equine tendon [8], and discriminate age in human tendon [9]. In addition, changes in ultrasound RF spectra with insonation angle in bovine tendon have been reported [10].

To date, methods for computationally quantifying the amount of disorganization, using ultrasound, between persons with and without tendinopathy have not been published. Quantification of this structural appearance through ultrasound promises to be an exceptional tool for diagnosing, prognosing, or measuring changes in tendon organization over time or in response to an intervention. In this paper, we propose a classification algorithm based on linear discriminant analysis (LDA) of several parameters derived from the spatial frequency spectrum. The goal of this work is to implement and test the classifier on a group of subjects experiencing symptoms consistent with tendinopathy compared to a control group.

Ultrasound RF data [11]–[15] and image texture analysis [16]–[20] have been used extensively to classify tissues for a variety of applications. The outcome of these analyses varied based on the ability to classify signal and/or image patterns, notably speckle structure. The main requirement for implementing a classification algorithm is measurable order in the underlying scattering structure. If the subresolution scatterers comprising tissue are located randomly, the speckle pattern will depend on the physical properties of the transducer and the beamforming parameters rather than the tissue structure [21]. For anisotropic scattering media, the correlation length of the speckle pattern will change depending on the orientation of the scatterers to the transducer [22], and may indicate underlying order of the tissue.

Previous attempts to classify tissue often used parameters derived directly or indirectly from the second-order statistics

Manuscript received September 20, 2007; revised October 24, 2007. This work was supported in part by the University of Nebraska Agricultural Research Division and in part by the Layman Foundation. *Asterisk indicates corresponding author.*

*G. R. Bashford is with the Department of Biological Systems Engineering, University of Nebraska-Lincoln, 230 L. W. Chase Hall, Lincoln, NE 68583 USA (e-mail: gbashford2@unl.edu).

N. Tomsen was with the Department of Biological Systems Engineering, University of Nebraska, Lincoln, NE 68583 USA. He is now with the College of Medicine, University of Iowa, Iowa City, IA 52240 USA.

S. Arya is with the Division of Biokinesiology and Physical Therapy, University of Southern California, Los Angeles, CA 90089 USA

J. M. Burnfield is with the Movement Sciences Center, Institute for Rehabilitation Science and Engineering, Madonna Rehabilitation Hospital, Lincoln, NE 68506 USA.

K. Kulig is with the Division of Biokinesiology and Physical Therapy, School of Dentistry, Department of Orthopaedic Surgery, Keck School of Medicine, University of Southern California, Los Angeles, CA 90089 USA.

Color versions of one or more of the figures in this paper are available online at http://ieeexplore.ieee.org.

Digital Object Identifier 10.1109/TMI.2007.912389

of the speckle pattern. Some of these functions include the co-occurrence matrix [23] and the spatial autocorrelation [22]. Methods using the frequency dependence of the backscatter power spectrum have also been applied [24], [25]. The autocorrelation function is related to the squared norm of the Fourier spectrum through the Wiener–Khinchin theorem, and thus methods using the Fourier transform have also been studied. Tuthill *et al.* [26] proposed a quantitative method using parameters derived from a moment analysis of the spatial frequency spectrum. Differentiating healthy from abnormal tendon tissue using this approach was found to be possible. Later, Liu *et al.* [27] derived a generalized theory for relating 2-D ultrasound signal spectra to the microstructure of tissue.

In clinical applications such as surgical repair or rehabilitation, quantifying the level of tendon structure disorganization would be advantageous for comparison of tissue health over time. This study aims to extend the results of previous researchers by using a conventional classifier algorithm, in particular linear discriminant analysis (LDA), on parameters derived from a filtered version of the spatial frequency spectrum.

Motivation for this study originated from visual inspection of the speckle pattern of a healthy tendon contrasted with the speckle pattern of subjects with symptoms characteristic of tendinopathy. Healthy tendon structure observed in ultrasound images results in a characteristic banded anisotropic speckle pattern with increased correlation length in the lateral dimension. It was hypothesized that these patterns would be marked by a spectrum with stronger magnitude components and narrower spatial bandwidths, near the fundamental frequency of the light-dark pattern, as compared with speckle patterns observed on damaged tendon. It was also hypothesized that spatial frequencies observed within healthy and unhealthy tendons in ultrasound images would vary sufficiently to enable use as a method for discriminating and categorizing between such groups.

LDA is a method for classification of data by finding the linear combination of features (discriminant functions) that best separate two or more classes of objects [28]. This tool can be used when the underlying probability distribution of the parameters are not known, and is useful as an initial classifier if the data do not suggest otherwise. For the present study, the two classes were defined to be those subjects reporting tendinopathy and a control group. Since the underlying speckle pattern may indicate damage in the tendon, it was hypothesized that separating tendons recorded from persons with and without tendinopathy might be accomplished through parameters derived from the spatial frequency spectra obtained from the two groups. Our objective, therefore, was to identify parameters from the spatial frequency spectrum that would increase accuracy of distinguishing between normal and abnormal tendon structure using LDA, with a long-term goal of providing a tool that can be used to quantify the degree of tendon health.

II. Materials and Methods

A. Subjects

Twenty males (age 20–40 years) with and without Achilles tendinopathy were recruited for this study. Subjects were divided into two groups determined by the presence or absence of Achilles tendinopathy (Tendinopathy group: $n = 10$; Control group: $n = 10$). Achilles tendinopathy was confirmed via a clinical history of Achilles tendon pain lasting a minimum of six weeks and the presence of pain in the Achilles tendon with palpation and walking [29]. Achilles tendinopathies were likely of traumatic origin as all participants were young and active without history of systemic collagen disease.

B. Procedures

The Institutional Review Boards at the University of Nebraska-Lincoln (UNL), the University of Southern California (USC), Los Angeles, and Madonna Rehabilitation Hospital, Lincoln, NE, granted approval for this study. Ultrasound images were gathered at USC. Informed consent was obtained from all subjects prior to the data collection in accordance with the IRB protocol. A questionnaire was administered to each individual scanned, for clinical history purposes and to identify subjects with diagnosed tendinopathy or other pathology. The same sonographer (S. Arya) scanned bilateral Achilles tendons for all subjects. B-mode ultrasound images were acquired with a commercial ultrasound scanner (Sonoline Antares, Siemens Medical Solutions USA Inc., Malvern, PA). A small-parts transducer (VFX 13–5 linear transducer, 11 MHz center frequency) was used with the musculoskeletal (MSK) preset, corresponding to a depth of 3.0 cm, with transmit foci of 1.0 and 1.5 cm. Care was taken to adjust the angle of the transducer for each image to ensure that the resultant image provided the brightest appearance of tendon structure thereby minimizing the possibility of introducing a position artifact [30]. The first 10 subjects recruited were imaged twice, on separate days, to assess intersession reliability of the imaging parameters.

C. Image Analysis and Parameter Extraction

The scans were digitally stored on the ultrasound machine as scanner-compressed JPEG intensity images, and the image data were imported into MATLAB (Mathworks, Natick, MA) for frequency analysis. Custom MATLAB code was created to allow for the selection of a region of interest (ROI) for each image analyzed. The ROI was selected by measuring 1.0 cm from the most proximal visible point of the calcaneous, using this point as the bottom left ROI polygon vertex. The ROI was a user-defined polygon with arbitrary number of sides. Within the ROI, 32×32 pixel kernels were extracted. Every possible kernel contained within the ROI boundary was used (see Fig. 1). The kernels were allowed to overlap; that is, processing was done with a sliding window rather than block windows.

The individual kernels were processed in the following manner. First, to increase frequency resolution, the data were zero-padded in both dimensions to a 128×128 size. Second, to suppress low spatial frequencies within the kernel, a 2-D highpass filter was applied with radial frequency response

$$H(p) = 1 - e^{-\alpha p} \tag{1}$$

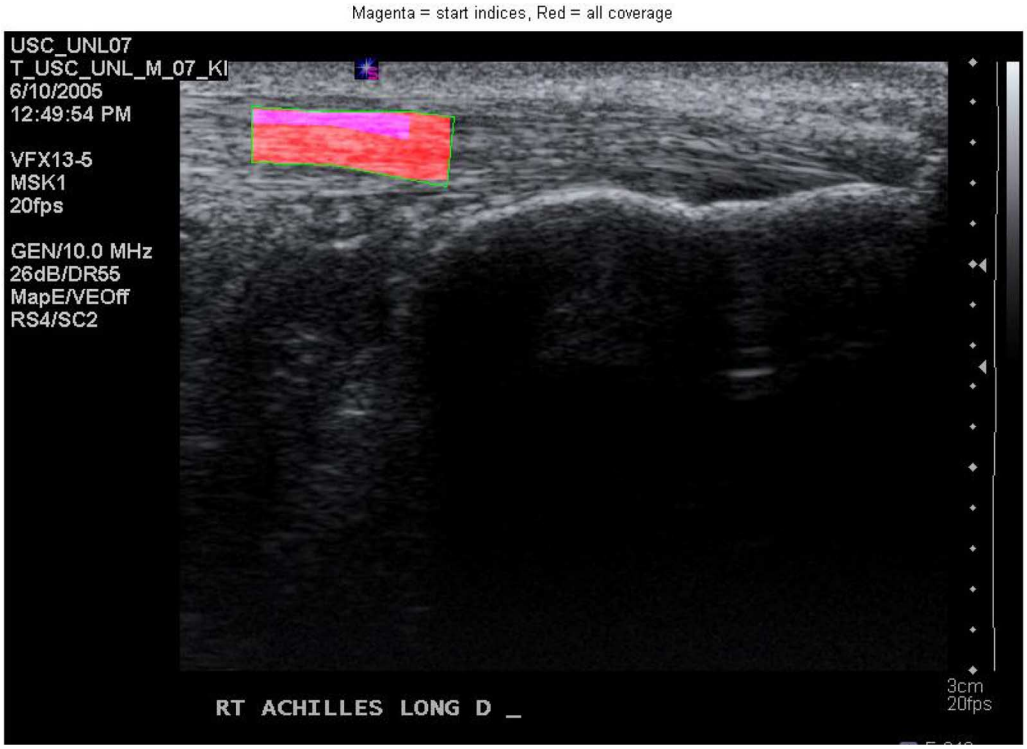

Fig. 1. Example ROI polygon selection. Upper left shaded portion indicates upper left vertex of all 32 × 32 kernels within the ROI. Complete shaded portion indicates union of all kernel pixels.

TABLE I
SPATIAL FREQUENCY PARAMETERS

Parameter #	Parameter Name	Description
1	Peak Spatial Frequency	Distance from origin to spatial frequency peak of greatest amplitude on 2-D FFT spectrum
2	P6 Width	Average of horizontal and vertical -6 dB widths of greatest amplitude spatial frequency peak on 2-D FFT spectrum
3	Q6 Factor	Ratio of Peak Spatial Frequency to P6 Width
4	Mmax	Value of the maximum point of amplitude on 2-D FFT
5	Mmax Percent	Ratio of Mmax to the total intensity of pixels in the 2-D FFT
6	Sum	Sum of intensities of original image kernel pixels
7	Axis Ratio*	Major-to-minor axis ratio of ellipsoidal fit 16 X 16 center pixel region of 2-D FFT
8	Ellipse Rotation*	Rotation from vertical axis of ellipsoid fit to 2-D FFT

*indicates parameter used by Tuthill et al [26].

where α is a user-adjustable bandwidth parameter. The half-power cutoff frequency ρ_c of this filter is

$$p_c = \frac{1n\left(\sqrt{2}/(\sqrt{2}-1)\right)}{\alpha} \cong \frac{1.23}{\alpha}. \tag{2}$$

The rationale for highpass filtering is as follows. We have found that applying no highpass filtering or weak highpass filtering results in greater errors in the discrimination algorithm, since the peak spatial frequency (Parameter 1 in Table I), is almost always at or near the spectrum origin (zero-frequency) without filtering. Central to this algorithm is the ability to detect the presence of a strong spatial frequency component not located at the spectrum origin. In the present study, two different values of α are considered: 5.0 (corresponding to a cutoff frequency of 0.25 mm^{-1}) and 1.0 (corresponding to a cutoff frequency of 1.23 mm^{-1}). After visual inspection of many tendon images and spectra, we have seen that strong frequency components between about 1.5 and 2.5 mm^{-1} are common in asymptomatic subjects.

After processing, eight parameters from the spatial frequency spectrum were extracted. The parameters were chosen after visually comparing many images between asymptomatic subjects and subjects experiencing tenalgia. As noted in Section I, one of the distinguishing features of an asymptomatic subject is a strong spatial frequency component corresponding

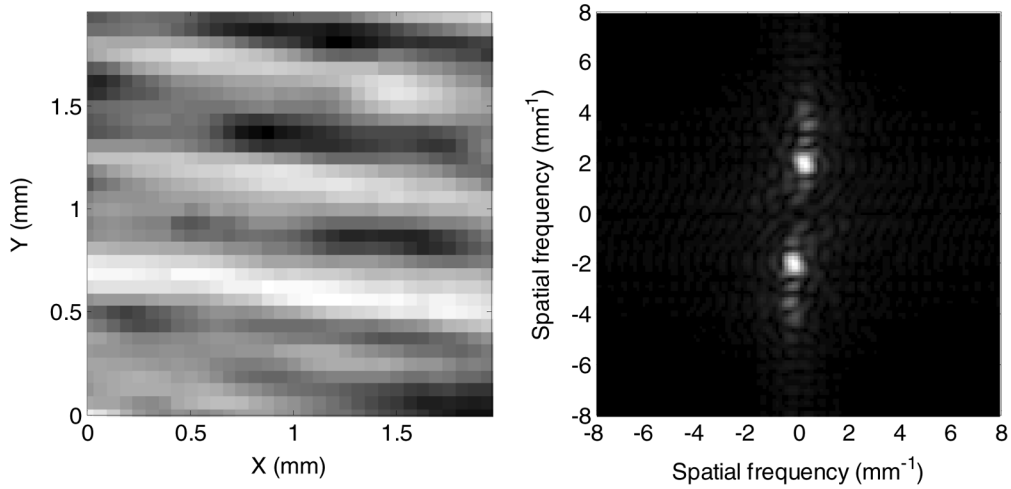

Fig. 2. Example image kernel and spatial frequency spectrum. Left, typical 32 × 32 pixel kernel within the Achilles tendon of a control subject. Right, spatial frequency spectrum obtained by taking the 2-D FFT of the left image. Note the strong spatial frequency components around 2.0 mm−1.

TABLE II
EXPERIMENTAL VARIABLES USED IN ANALYSES

	Experiment			
	1	2	3	4
Highpass Filter Setting (α)	5.0	1.0	1.0	1.0
Discriminant Parameters	All	All	All	Optimized (1-5)
Discriminant Analysis Type	LDA	LDA	QDA	LDA

to the anisotropic speckle bands observed in the images. It is important to note that the individual bands do not correspond to individual fibrils, but rather to a coherent sum of reflections from many fibrils. In contrast, the speckle pattern from subjects experiencing tenalgia exhibits greater disorganization manifested in a more isotropic frequency spectrum. An example kernel and spatial frequency spectrum is shown in Fig. 2. A description of the image parameters along with calculation instructions is shown in Table I. Six of the eight image parameters were chosen in an attempt to capture the difference between the strong-amplitude, narrow-bandwidth features observed in normal subjects and the comparatively weaker-amplitude, broader-bandwidth features observed in subjects with tendinopathies. The other two parameters were chosen to be the same as those suggested by Tuthill *et al.* [26].

D. Algorithm Formation

An $N \times 8$ matrix was formed where each of the eight columns was a parameter, and each of the N rows contained an observation of the eight parameters extracted from one of the N image kernels. Training sets and testing sets were formed by vertically concatenating matrices from appropriate subjects. The larger matrices were entered into custom LDA code obtained from the Mathworks user group website [31]. The resulting discriminant functions were used to categorize the test kernels as belonging to the tendinopathy group or the normal group.

Two experimental variables were adjusted in the set of experiments performed (see Table II). The first variable adjusted was the highpass filter setting ($\alpha = 1.0, \alpha = 5.0$) discussed previously. The second variable was the discriminant parameters included from Table I. A batch process was implemented to test all possible subsets of the eight parameters by a combinatorial analysis. The best parameter subset was judged to be that which gave the highest average true classification percentage in the main diagonal of the confusion matrix. In addition to these variables, one additional experiment tested classification accuracy using a quadratic discriminant analysis (QDA), in which the decision boundary may assume a hyperquadric surface, to determine if the parameters are better separated along nonlinear boundaries.

For each experiment, a traditional leave-one-out (LOO) analysis was performed. In this procedure, a single subject comprises the test set, with the remaining subjects comprising the training set. This step is repeated with each subject. The averaged results were used to form a confusion matrix. The confusion matrix is a representation of the summation of all correct kernel categorizations from the 10 control subject tendon images and the 10 tendinopathy subject tendon images over the incorrect kernel categorizations. A percentage of the kernels categorized correctly or incorrectly for each group results. Additionally, for each experiment the individual subject results were examined for consistency and possible anomalies.

III. RESULTS

A. Experiment 1: Eight Parameter LDA, α = 5.0

The first experiment performed used all eight parameters and a highpass filter value of α = 5.0. The results are shown as a confusion matrix in Table III.

TABLE III
CONFUSION MATRIX OF LOO ANALYSIS FROM LDA WITH $\alpha = 5.0$

		Predicted Class	
		Control	Tendinopathy
Actual Class	Control	83.4%	16.6%
	Tendinopathy	19.8%	80.2%

TABLE IV
CONFUSION MATRIX OF LOO ANALYSIS FROM LDA WITH $\alpha = 1.0$

		Predicted Class	
		Control	Tendinopathy
Actual Class	Control	80.3%	19.7%
	Tendinopathy	15.1%	84.9%

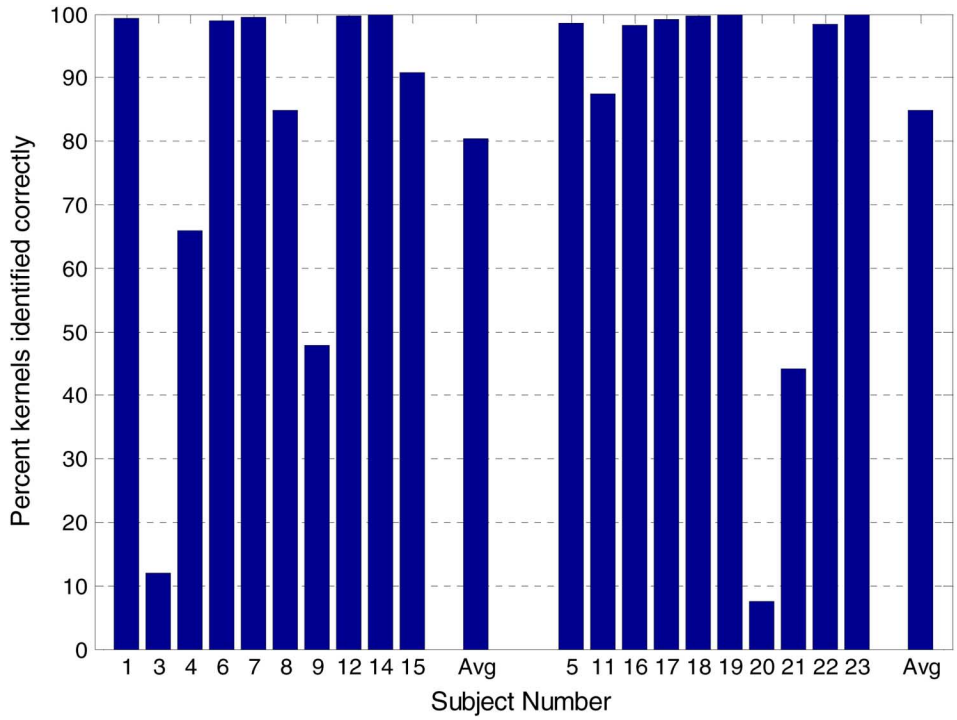

Fig. 3. Individual subject results from LOO analysis with $\alpha = 1.0$ using LDA. Left group (1 to 15), controls; right group (5 to 23), tendinopathy.

B. Experiment 2: Eight Parameter LDA, α = 1.0

In the second experiment, the filter value was changed to 1.0, which attenuates the lower spatial frequencies to a greater degree. The results are shown in the confusion matrix in Table IV. An example of the individual subject results is shown in Fig. 3.

C. Experiment 3: Eight Parameter QDA, α = 1.0

In experiment 3, the same settings and procedures as described in the second experiment were used except QDA was substituted for LDA. The results are shown in the confusion matrix in Table V.

D. Experiment 4: Optimized Parameter LDA, $\alpha = 1.0$

For experiment 4, custom code was written that tested all combinations of the eight parameters that were extracted from spatial frequency information from each image kernel. All combinations were tested to find the optimum grouping of parameters for the greatest accuracy in categorization of images. The results indicated that using five parameters led to highest accuracy: peak spatial frequency, P6 Width, Q6 Factor, Mmax, and Mmax Percent (parameters 1–5 in Table I). The results in the confusion matrix are shown in Table VI.

E. Intersession Reliability Experiment

To assess test–retest (intersession) reliability, a comparison of classification results derived from Achilles tendon images recorded during two separate sessions by the same sonographer was performed for a subgroup of 10 subjects $(n = 8 \text{ control}, n = 2 \text{ tendinopathy})$. New ROIs were selected from each of the separate session images at a fixed

TABLE V
CONFUSION MATRIX OF LOO ANALYSIS FROM QDA WITH $\alpha = 1.0$

		Predicted Class	
		Control	Tendinopathy
Actual Class	Control	82.2%	17.8%
	Tendinopathy	21.1%	78.9%

TABLE VI
CONFUSION MATRIX OF LOO ANALYSIS FROM OPTIMIZED PARAMETER LDA WITH $\alpha = 1.0$

		Predicted Class	
		Control	Tendinopathy
Actual Class	Control	81.0%	19.0%
	Tendinopathy	16.0%	84.0%

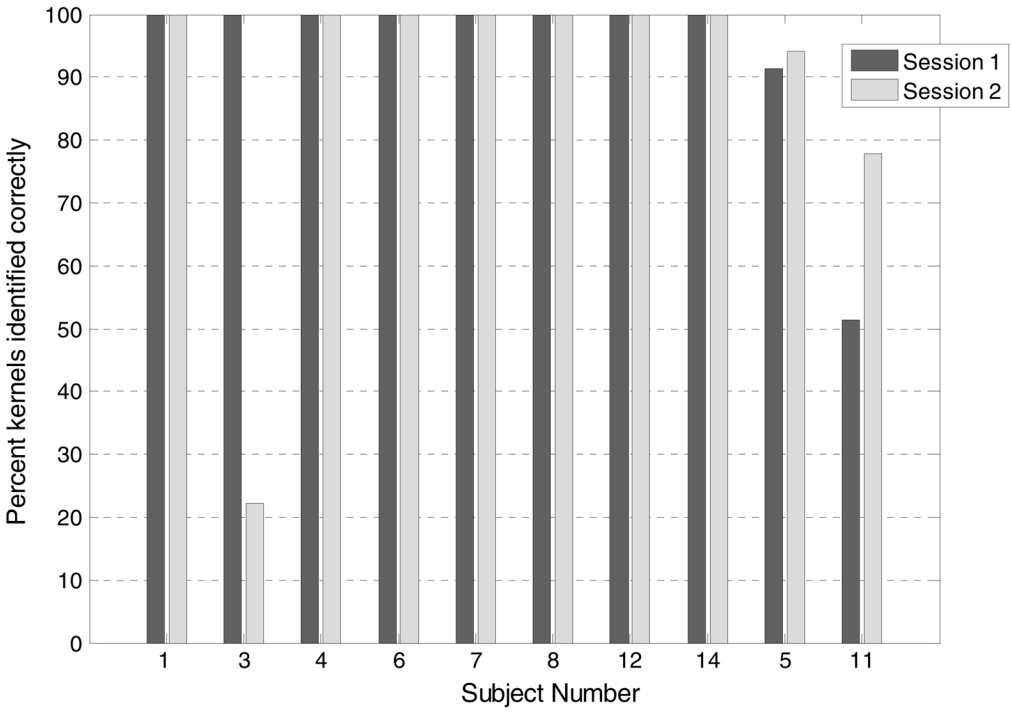

Fig. 4. Comparison of Imaging Session Data.

distance of 1.0 cm from the calcaneous by the same sonographer (SA) who selected the first set of ROIs. An adjustment to the LOO analysis was made by using a test set consisting of both images from the same subject (two imaging sessions). The training set included the image data from all other subjects. The new analysis was tested on the image kernels from both session images. The results are displayed in Fig. 4. Except for subject 3, the repeatability is observed to be very good. The intraclass correlation [ICC(2,1)] without subject 3 is 0.73 [with subject 3 $\mathrm{ICC}(2,1) = 0.12$].

IV. DISCUSSION

The overall purpose of this research was to develop an algorithm, based on LDA, which could be used to accurately classify and quantify the degree of tendon fibril organization, or the lack of, evident in ultrasound images. To date, the degree of disorganization has primarily been described qualitatively using phrases such as "localized regions of hypoechocity" or "darkness" to convey the presence of pathology. Our goal was to develop a classification system which did not rely, solely, on human observation. To accomplish this goal, we selected for comparison tendons from two groups (those with tendinopathy and asymptomatic controls) which were expected to differ notably in organizational structure. The overall level of accuracy in differentiating between the two groups was greater than 80%, suggesting that this is a promising technique for classifying tendon structure by image analysis. Slight increases in classification accuracy were observed by varying the filter and number of parameters used, but none of the results of experiments 1–4 were significantly different from one another.

Moreover, the kernels of individual images were categorized correctly more than 80% of the time. Only a few of the images were categorized with low accuracy. Consistently within our experiments, the tendon images from subjects 3, 9, 20, and 21 were categorized with low accuracy regardless of the experimental variables used to create the algorithm for testing these images.

One factor that may have contributed to the incorrect classification of subjects was the presence of underlying pathology that was not discernable through the clinical history and symptomatology. It is likely that the degree of pathology present in the tendons of subjects classified both as control and especially tendinopathy groups actually encompassed a spectrum of tendon health conditions, and therefore a range of spatial frequency characteristics. To determine the actual level of pathology present in the tendon, further work comparing findings from a histopathological analysis of harvested tendon tissue to those obtained from our image analyses is required.

However, insights can be gained from further analysis of the clinical histories of subjects whose tendons were "incorrectly" classified. Specifically, subject 20, an individual presenting with symptoms consistent with tendinopathy, was classified as having a relatively small portion of tendinopathy kernels (ranging from approximately 3%–8% across techniques). This subject reported onset of symptoms only four months prior to imaging. Similarly, subject 21, who also presented with symptoms consistent with tendinopathy, was classified as having a relatively small portion of tendinopathy kernels during the analysis (ranging from approximately 30%–44% across techniques). This individual had been experiencing sporadic Achilles tendon pain for only 1.5 years prior to the imaging session. With the exception of subject 23, who had also experienced pain for approximately 1.5 years prior to imaging, all other subjects with tendinopathy had longer histories of tendon pain ($\min. = 3$ years, $\max. = 26$ years, $\mathrm{mean} = 12.6$ years, $\mathrm{median} = 12.5$ years).

The duration of time tendon pain is present may relate to the amount of change taking place within tendon fibril structure. Complete changes in the tendon fibril structure may not have fully taken place in subjects 20 and 21, leading to the possibility that images of these subjects correlate more closely to control subjects than to the tendinopathy subjects for which they were initially grouped because of the pain.

It is also possible that disruption of tendon fibril organization may exist (such as xanthomas), yet a patient will not demonstrate clinical symptoms (e.g., pain, swelling). For example, the algorithms classified subjects 3 and 9 in the control group as primarily having kernels associated with tendinopathy, yet they did not clinically present with this diagnosis. Finally, error in image acquisition could have contributed to this categorization. Collectively, the paradoxical findings reinforce the need for subsequent research relating tissue histopathology to findings from the algorithm analysis of tendon structure as well as analyses of images from repeated measures.

For intersession reliability, the results suggest that except for subject 3, images from both sessions were categorized consistently. The reason for the modest increase in accuracy is thought to be due to the new ROI selection protocol. The ROIs used in the intersession experiment were defined to be a specific distance from a known body landmark and encompassed a smaller area of the tendon image than the ROIs used previously. The results show that the image protocol was consistent in imaging subjects. This conclusion is true in all cases except in subject 3 who was categorized wrongly by the original algorithm. Further study into the clinical background and correlation of subject images from different sessions shows promise in greatly increasing the accuracy of categorizing tendon through the creation of a modified algorithm.

Based on the current findings, a number of future directions for this work may be suggested to improve the accuracy of the algorithm classification. Possible strategies include developing additional spatial frequency parameters, testing alternative classifiers such as neural nets or soft computing techniques, and evaluating additional clinical groups, such as runners or spinal cord injury subjects. Additionally, validation of algorithm classification to histopathological findings of select tendon tissues may provide valuable insights for refining the algorithms. Also, instrumentation designed to combine the method proposed here with detection of angle-dependent echogenicity suggested by Garcia *et al.* [8] may prove especially helpful in detecting and quantifying mechanical damage to tendon. Finally, experimenting with methods of image acquisition may shed additional light on the issue.

V. Summary

The development of an algorithm for classification of tendon tissue into two groups has been successfully demonstrated through the use of spatial frequency parameters and LDA. Several changes in experimental variables led to an algorithm with greater than 80% accuracy in categorizing tendon tissue between tendinopathy and normal tendon groups. Correlation in categorization was observed through comparing images taken from different imaging sessions, suggesting that the algorithm was consistent within the same tendon and that the algorithm was robust across imaging sessions. Improved accuracy was observed within the image session comparison experiment, and reasons for this increase are currently being investigated and allow for a wide direction of future investigations. Additionally, potential confounding clinical factors (e.g., the duration of pain) were identified that provide fruitful ground for further research. This work presents the first in a series of steps to allow for more accurate classification and quantification of the degree of tendon disorganization. Future work will focus on improving classification accuracy and validation of classification via histopathological confirmation.

References

[1] I. R. Telford and C. F. Bridgman, , I. R. Telford and C. F. Bridgman, Eds., "Connective tissue I-cells and fibers," in *Introduction to Functional Histology*, 1st ed. New York: Harper Collins, 1995, pp. 79–98.

[2] R. R. Bleakney, C. Tallon, J. K. Wong, K. P. Lim, and N. Maffulli, "Long-term ultrasonographic features of the achilles tendon after rupture," *Clin. J. Sport Med.*, vol. 12, no. 5, pp. 273–278, 2002.

[3] N. Ofer, S. Akselrod, M. Nyska, M. Werner, E. Glaser, and S. Shabat, "Motion-based tendon diagnosis using sequence processing of ultrasound images," *J. Orthop. Res.*, vol. 22, no. 6, pp. 1296–1302, 2004.

[4] D. J. Connolly, L. Berman, and E. G. McNally, "The use of beam angulation to overcome anisotropy when viewing human tendon with high frequency linear array ultrasound," *Br. J. Radiol.*, vol. 74, no. 878, pp. 183–185, 2001.

[5] B. K. Hoffmeister, A. K. Wong, E. D. Verdonk, S. A. Wickline, and J. G. Miller, "Comparison of the anisotropy of apparent integrated ultrasonic backscatter from fixed human tendon and fixed human myocardium," *J. Acoust. Soc. Amer.*, vol. 97, no. 2, pp. 1307–1313, 1995.

[6] R. O. Bude, R. S. Adler, D. R. Bassett, D. M. Ikeda, and J. M. Rubin, "Heterozygous familial hypercholesterolemia: Detection of xanthomas in the achilles tendon with US," *Radiology*, vol. 188, no. 2, pp. 567–571, 1993.

[7] T. Koivunen-Niemela, A. Alanen, and J. Viikari, "Sonography of the achilles tendon in hypercholesterolaemia," *J. Internal Med.*, vol. 234, pp. 401–405, 1993.

[8] T. Garcia, W. J. Hornof, and M. F. Insana, "On the ultrasonic properties of tendon," *Ultrasound Med. Biol.*, vol. 29, no. 12, pp. 1787–1797, 2003.

[9] D. Yi-Chun, C. Yung-Fu, L. Chi-Jeng, L. Yu-Ching, and C. Tainsong, The application of quantitative ultrasound (QUS) on study of aging effects of achilles tendons pp. 6344–6347, 2005.

[10] M. R. Holland, S. H. Lewis, C. S. Hall, A. E. Finch-Johnston, S. M. Handley, K. D. Wallace, A. P. D'sa, D. M. Prater, J. E. Perez, and J. G. Miller, "Effects of tissue anisotropy on the spectral characteristics of ultrasonic backscatter measured with a clinical imaging system," *Ultrason. Imag.*, vol. 20, no. 3, pp. 178–190, 1998.

[11] P. Stetson and G. Sommer, "Ultrasonic characterization of tissues via backscatter frequency dependence," *Ultrasound Med. Biol.*, vol. 23, no. 7, pp. 989–996, 1997.

[12] W. C. Pereira, S. L. Bridal, A. Coron, and P. Laugier, "Singular spectrum analysis applied to backscattered ultrasound signals from in vitro human cancellous bone specimens," *IEEE Trans. Ultrason. Ferroelect. Freq. Control*, vol. 51, no. 3, pp. 302–312, 2004.

[13] F. L. Lizzi, M. Greenebaum, E. J. Feleppa, M. Elbaum, and D. J. Coleman, "Theoretical framework for spectrum analysis in ultrasonic tissue characterization," *J. Acoust. Soc. Amer.*, vol. 73, no. 4, pp. 1366–1373, 1983.

[14] D. Savery and G. Cloutier, "High-frequency ultrasound backscattering by blood: Analytical and semianalytical models of the erythrocyte cross section," *J. Acoust. Soc. Amer.*, vol. 121, no. 6, pp. 3963–3971, 2007.

[15] M. Strowitzki, S. Brand, and K. V. Jenderka, "Ultrasonic radio-frequency spectrum analysis of normal brain tissue," *Ultrasound Med. Biol.*, vol. 33, no. 4, pp. 522–529, 2007.

[16] H. Yoshida, D. D. Casalino, B. Keserci, A. Coskun, O. Ozturk, and A. Savranlar, "Wavelet-packet-based texture analysis for differentiation between benign and malignant liver tumours in ultrasound images," *Phys. Med. Biol.*, vol. 48, pp. 3735–3753, 2003.

[17] J. Segyeong , S. Y. Yoon, K. M. Woo, and C. K. Hee, "Computer-aided diagnosis of solid breast nodules: Use of an artificial neural network based on multiple sonographic features," *IEEE Trans. Med. Imag.*, vol. 23, no. 10, pp. 1292–1300, Oct. 2004.

[18] E. K. Kerut, M. Given, and T. D. Giles, "Review of methods for texture analysis of myocardium from echocardiographic images: A means of tissue characterization," *Echocardiography*, vol. 20, no. 8, pp. 727–736, Nov. 2003.

[19] P. E. Aylward, B. N. Knosp, D. D. McPherson, D. A. Eltoft, C. E. Yurkonis, J. A. Bean, D. J. Skorton, and S. M. Collins, "Two-dimensional echocardiographic image texture analysis: Reduction of regional variability using polar coordinates," *Ultrason. Imag.*, vol. 7, no. 1, pp. 60–73, 1985.

[20] K. Wu, Y. Wang, Y. Pan, J. Zhang, B. Qian, and C. Chang, "Classifying uterine myoma and adenomyosis based on ultrasound image fractal and texture features," in *Conf. Proc. IEEE Eng. Med. Biol. Soc.*, 2005, vol. 2, pp. 1790–1793.

[21] R. F. Wagner, S. W. Smith, J. M. Sandrik, and H. Lopez, "Statistics of speckle in ultrasound b-scans," *IEEE Trans. Sonics Ultrason.*, vol. SU-30, no. 3, pp. 156–163, 1983.

[22] A. Derode and M. Fink, "Correlation length of ultrasonic speckle in anisotropic random media: Application to coherent echo detection," *J. Acoust. Soc. Amer.*, vol. 103, no. 1, pp. 73–82, 1998.

[23] U. Haberkorn, I. Zuna, A. Lorenz, H. Zerban, G. Layer, K. G. van, and U. Rath, "Echographic tissue characterization in diffuse parenchymal liver disease: Correlation of image structure with histology," *Ultrason. Imag.*, vol. 12, no. 3, pp. 155–170, 1990.

[24] M. L. Oelze, J. F. Zachary, and W. D. O'Brien, Jr., "Characterization of tissue microstructure using ultrasonic backscatter: Theory and technique for optimization using a gaussian form factor," *J. Acoust. Soc. Amer.*, vol. 112, no. 3, pt. 1, pp. 1202–1211, 2002.

[25] F. G. Sommer, P. Stetson, H. S. Chen, R. A. Stern, D. J. Rachlin, and A. Macovski, "Prospects for ultrasonic spectroscopy and spectral imaging of abdominal tissues," *J. Ultrasound Med.*, vol. 12, no. 2, pp. 83–90, 1993.

[26] T. A. Tuthill, J. M. Rubin, J. B. Fowlkes, D. A. Jamadar, and R. O. Bude, "Frequency analysis of echo texture in tendon," *Ultrasound Med. Biol.*, vol. 25, no. 6, pp. 959–968, 1999.

[27] T. Liu, F. L. Lizzi, J. A. Ketterling, R. H. Silverman, and G. J. Kutcher, "Ultrasonic tissue characterization via 2-D spectrum analysis: Theory and in vitro measurements," *Med. Phys.*, vol. 34, no. 3, pp. 1037–1046, 2007.

[28] R. O. Duda, P. E. Hart, and D. G. Stork, "Linear discriminant functions," in *Pattern Classification*, 2nd ed. New York: Wiley, 2001, ch. 5, pp. 215–281.

[29] L. G. Jozsa and P. Kannus, *Human Tendons: Anatomy, Physiology, and Pathology*. Champaign, IL: Human Kinetics, 1997.

[30] B. D. Fornage, "The hypoechoic normal tendon: A pitfall," *J. Ultrasound Med.*, vol. 6, pp. 19–22, 1987.

[31] M. Kiefte, Discriminant Analysis Toolbox v. 0.3.. [Online]. Available: http://www.mathworks.com/matlabcentral/fileexchange